Controllable asymmetric double well and ring potential on an atom chip

S. J. Kim,[1] H. Yu,[1,2] S. T. Gang,[1] D. Z. Anderson,[2] and J. B. Kim[1,*]

[1]*Department of Physics Education, Korea National University of Education, Chung-Buk 363-791, Republic of Korea*

[2]*Department of Physics and JILA, University of Colorado, Boulder, Colorado 80309-0440, USA*

(Received 31 May 2015; revised manuscript received 28 November 2015; published 4 March 2016)

We have constructed an asymmetric matter-wave beam splitter and a ring potential on an atom chip with Bose-Einstein condensates using radio-frequency dressing. By applying rf field parallel to the quantization axis in the vicinity of the static trap minima added to perpendicular rf fields, versatile controllability on the asymmetry of rf-dressed potentials is realized. Asymmetry of the rf-induced double well is controlled over a wide range without discernible displacement of each well. Formation of an isotropic ring potential on an atom chip is achieved by compensating the gradient due to gravity and inhomogeneous coupling strength. In addition, position and rotation velocity of a BEC along the ring geometry are controlled by the relative phase and the frequency difference between the rf fields, respectively.

DOI: 10.1103/PhysRevA.93.033612

I. INTRODUCTION

Microscopic magnetic traps utilizing an atom chip are of interest for the study of neutral atoms and Bose-Einstein condensates (BECs) since they offer a degree of design flexibility, precise control over the trapped atoms, and feasibility of integration of atom-optical elements [1]. Introducing radio-frequency (rf) radiation to modify the static potential improves the design flexibility of the atom trapping geometry [2–7]. Adiabatic rf-dressed potentials have the benefit of being smooth and offer long phase coherence times while maintaining high confinement during flexible deformation of the trap geometry [4]. The most common geometries for rf-dressed adiabatic potentials are double wells and ring potentials [4–7]. The rf-induced double well acts as a matter-wave beam splitter and thus has been used for atom interferometry [8,9] utilized for the study of precision measurement [10,11], phase dynamics [12,13], squeezed and entangled states [14–16], and superfluidity [17], etc. Since the contrast and the coherence time of the interferometer depend on the balance of the two wells, precise control over the asymmetry of the double well is very important [8,15]. Trap asymmetry can be used as a means to shift the relative phase of the interferometer arms [18] and as a means of setting the bias of a Josephson junction for superfluidity studies [17,19,20].

Ring-shaped traps have been also studied [5,7,21–28], since the geometry can be used to construct multiply connected systems with behavior not found in other types of traps [25,29,30]. Such ring traps also have practical applications for Sagnac interferometry for inertial sensing [18,25] and are also of fundamental interest as an analog of the superconducting quantum interference device (SQUID) [26,31] and for the study of superfluidity and quantization of angular momentum [22,27,28,32,33], etc. Even though a ring potential on an atom chip was suggested in Ref. [4], it was not realized due to gravity and the inhomogeneous coupling strength of the rf field [5].

In this paper, we report on the realization of a controllable asymmetric matter-wave beam splitter and a ring potential on an atom chip. The theory of the asymmetric rf-induced potentials is discussed, and the formation of various geometries is explained. Experimental results showing the versatility of the rf-induced potentials are presented. The double-well asymmetry is controlled and is investigated by measuring the relative atom number between the two wells. For a ring potential, homogeneity was obtained by adjusting the asymmetry to compensate for the inhomogeneity. In addition, a rotation scheme to introduce angular momentum into a ring BEC is also investigated.

II. THEORY OF THE ASYMMETRIC RF-INDUCED POTENTIALS

A. Analytical calculation of the rf-dressed potential

Since the coupling between a static field and rf fields critically depends on the vector characteristics of the fields, controlling this is the key to the versatility of the rf-induced potentials [4]. To achieve this, we create the rf-dressed potentials by combining a static Ioffe magnetic trap $\mathbf{B}_S(\mathbf{r})$ with a three-component rf field $\mathbf{B}_{\rm rf}$ having frequency $\omega_{\rm rf}/2\pi$ and relative phase shifts δ and δ_z.

$$\begin{aligned}\mathbf{B}_S(\mathbf{r}) &= Gx\mathbf{e}_x - Gy\mathbf{e}_y + B_I\mathbf{e}_z \\ &= G\rho\cos\phi\mathbf{e}_x - G\rho\sin\phi\mathbf{e}_y + B_I\mathbf{e}_z, \end{aligned} \tag{1}$$

$$\begin{aligned}\mathbf{B}_{\rm rf} &= B^A_{\rm rf}\mathbf{e}_x\cos(\omega_{\rm rf}t) + B^B_{\rm rf}\mathbf{e}_y\cos(\omega_{\rm rf}t-\delta) \\ &\quad + B^z_{\rm rf}\mathbf{e}_z\cos(\omega_{\rm rf}t-\delta_z). \end{aligned} \tag{2}$$

Here G is the gradient of the static trap; B_I is the magnitude of the Ioffe field; $\rho=\sqrt{x^2+y^2}$ and $\phi=\arctan(y/x)$ in cylindrical coordinates. $B^A_{\rm rf}$, $B^B_{\rm rf}$, and $B^z_{\rm rf}$ are the amplitudes of the rf fields and t is time. Following [4], the corresponding rf-induced potentials can be written as

$$V_{ad}(\mathbf{r}) = m_F g_F \mu_B \sqrt{\Delta(\mathbf{r})^2+\Omega(\mathbf{r})^2}, \tag{3}$$

where m_F is the magnetic quantum number, g_F is the g factor of the hyperfine state, and μ_B is the Bohr magneton. The detuning $\Delta(\mathbf{r})$ and the coupling term $\Omega(\mathbf{r})$ are given by

$$\Delta(\mathbf{r}) = |\mathbf{B}_S(\mathbf{r})| - \frac{\hbar\omega_{rf}}{|g_F\mu_B|}, \tag{4}$$

*jbkim@knue.ac.kr

$$\Omega(\mathbf{r}) = \frac{|\mathbf{B}_{\rm eff}(\mathbf{r}) \times \mathbf{B}_S(\mathbf{r})|}{|\mathbf{B}_S(\mathbf{r})|}. \quad (5)$$

The effective rf field $\mathbf{B}_{\rm eff}(\mathbf{r})$ is calculated by applying rotation matrices with the angles $\alpha(\mathbf{r}) = \arctan[B_{S_y}(\mathbf{r})/B_{S_x}(\mathbf{r})]$ and $\beta(\mathbf{r}) = \arctan[\sqrt{B_{S_x}^2(\mathbf{r}) + B_{S_y}^2(\mathbf{r})}/B_{S_z}(\mathbf{r})]$ to the rf field $\mathbf{B}_{\rm rf}$ as

$$\begin{aligned}\mathbf{B}_{\rm eff}(\mathbf{r}) = {} & R_y[\beta(\mathbf{r})]R_z[\alpha(\mathbf{r})]\begin{pmatrix} B_{\rm rf}^A \\ 0 \\ 0 \end{pmatrix} \\ & + R_z\left[\frac{-g_F}{|g_F|}\delta\right]R_y[\beta(\mathbf{r})]R_z[\alpha(\mathbf{r})]\begin{pmatrix} 0 \\ B_{\rm rf}^B \\ 0 \end{pmatrix} \\ & + R_z\left[\frac{-g_F}{|g_F|}\delta_z\right]R_y[\beta(\mathbf{r})]R_z[\alpha(\mathbf{r})]\begin{pmatrix} 0 \\ 0 \\ B_{\rm rf}^z \end{pmatrix}, \quad (6)\end{aligned}$$

where the rotation matrices $R_y[\beta(\mathbf{r})]R_z[\alpha(\mathbf{r})]$ for diagonalization depend on the local z axis,

$$\begin{aligned}R_y[\beta(\mathbf{r})]R_z[\alpha(\mathbf{r})] = {} & \begin{pmatrix} \frac{B_I}{\sqrt{B_I^2+G^2\rho^2}} & 0 & \frac{-G\rho}{\sqrt{B_I^2+G^2\rho^2}} \\ 0 & 1 & 0 \\ \frac{G\rho}{\sqrt{B_I^2+G^2\rho^2}} & 0 & \frac{B_I}{\sqrt{B_I^2+G^2\rho^2}} \end{pmatrix} \\ & \times \begin{pmatrix} \cos\phi & -\sin\phi & 0 \\ \sin\phi & \cos\phi & 0 \\ 0 & 0 & 1 \end{pmatrix}. \quad (7)\end{aligned}$$

In this paper, later equations are calculated in the case of $B_{\rm rf}^A = B_{\rm rf}^B = B_{\rm rf}$ for simplicity, though controlling the ratio of $B_{\rm rf}^A$ and $B_{\rm rf}^B$ can be used to obtain more versatility on the rf-dressed potentials such as rotation of the double wells around the z axis [10,25]. We also restrict later calculations to negative detuning, $\omega < |g_F\mu_B|B_I/\hbar$, which is adequate for our experimental situation.

B. Rf-dressed potentials with two-component rf field ($B_{\rm rf}^z = 0$): Symmetric potentials

The coupling term for $B_{\rm rf}^z = 0$ can be calculated as

$$\begin{aligned}\Omega(\mathbf{r})^2 = {} & \frac{B_{\rm rf}^2}{4|\mathbf{B}_S(\mathbf{r})|^2}\{2B_I[B_I + |\mathbf{B}_S(\mathbf{r})|\sin\gamma] \\ & + G^2\rho^2[1 + \sin(2\phi)\cos\gamma]\}, \quad (8)\end{aligned}$$

where $\gamma = \frac{g_F}{|g_F|}\delta$ is the effective phase shift that depends on the sign of the Lande g factor [4].

Equation (8) simplifies to

$$\Omega(\mathbf{r})^2 = \frac{B_{\rm rf}^2}{4|\mathbf{B}_S(\mathbf{r})|^2}\left\{2B_I^2 + G^2\rho^2[1 \pm \sin(2\phi)]\right\}, \quad (9)$$

where the positive (negative) sign of the last term corresponds to $\delta = 0$ ($\delta = \pi$). Since the detuning term is rotationally symmetric, the coupling term dominates the determination of the geometry of the rf-dressed potential. Equation (9) allows us to manipulate a double-well potential.

For the case of a circularly polarized rf field, $\delta = \pi/2$ or $3\pi/2$, the coupling term Eq. (8) can be written as

$$\Omega(\mathbf{r})^2 = \frac{B_{\rm rf}^2}{4|\mathbf{B}_S(\mathbf{r})|^2}\{2B_I[B_I \pm |\mathbf{B}_S(\mathbf{r})|] + G^2\rho^2\}. \quad (10)$$

Here, the $\pm$ sign is decided by the effective phase shift γ. The sign is positive for $\gamma = \pi/2, -3\pi/2$ and negative for $\gamma = -\pi/2, 3\pi/2$. Since the detuning term and the coupling term are rotationally symmetric, the total rf-dressed potential is also rotationally symmetric. Consequently, in the area of $\rho \ll B_I/G$, the rf-dressed potential forms a ring potential with sufficient rf-field amplitude $B_{rf} > B_c$ for $\sin\gamma = 1$.

C. Rf-dressed potentials with three-component rf field ($B_{\rm rf}^z \neq 0$): Additional controllable asymmetry

From the coupling term $\Omega(\boldsymbol{r})^2$, an additional component on top of the symmetric potential without $B_{\rm rf}^z$ can be found as

$$\begin{aligned}\Omega(\mathbf{r})^2\big|_{B_{\rm rf}^z\neq 0} - \Omega(\mathbf{r})^2\big|_{B_{\rm rf}^z=0} = {} & \left[\frac{G\rho B_{\rm rf}^2}{2|\mathbf{B}_S(\mathbf{r})|}\right]^2 + \frac{GB_{\rm rf}}{2|\mathbf{B}_S(\mathbf{r})|^2}B_{\rm rf}^z \\ & \times\{\sin\delta_z[|\mathbf{B}_S(\mathbf{r})|y + B_I y\sin\delta + |\mathbf{B}_S(\mathbf{r})|x\cos\delta] \\ & - \cos\delta_z(B_I x - B_I y\cos\delta + |\mathbf{B}_S(\mathbf{r})|x\sin\delta)\}. \quad (11)\end{aligned}$$

Though the right side of Eq. (11) has a rotationally symmetric term $[G\rho B_{{\rm rf}^2/2}|\mathbf{B_S}(\mathbf{r})|]^2$, Eq. (11) describes the controllability of the asymmetry of the rf-dressed potentials. This rotationally symmetric term can be neglected in the area of $\rho \ll B_I/G$ or within our experimental situations, $B_{\rm rf}^z \ll B_{\rm rf}$. The symmetric term is neglected in the following equations for simplicity.

Equation (11) is reduced when $\delta_z = 0$ for double-well potentials to

$$\Omega(\mathbf{r})^2\big|_{B_{\rm rf}^z\neq 0} - \Omega(\mathbf{r})^2\big|_{B_{\rm rf}^z=0} = \frac{-GB_I B_{\rm rf}}{2|\mathbf{B}_S(\mathbf{r})|^2}B_{\rm rf}^z(x \mp y), \quad (12)$$

where $-$ and $+$ signs indicate $\delta = 0$ and π, respectively. The additional component following Eq. (12) shows the spatial gradient of the potential along the orientation of the rf-dressed double well, $x \mp y$. The gradient depends linearly on the amplitude of the rf field along the z axis $B_{\rm rf}^z$. Consequently, the nonzero $B_{\rm rf}^z$ increases the trap bottom of one well of the rf-dressed double-well potential while decreasing the other well's trap bottom. The increased (decreased) quantity can be controlled with $B_{\rm rf}^z$.

Equation (11) can also be written for a ring potential as ($\delta = \pi/2$)

$$\begin{aligned}\Omega(\mathbf{r})^2\big|_{B_{\rm rf}^z\neq 0} - \Omega(\mathbf{r})^2\big|_{B_{\rm rf}^z=0} = {} & \frac{-G(|\mathbf{B}_S(\mathbf{r})| + B_I)B_{\rm rf}}{2|\mathbf{B}_S(\mathbf{r})|^2} \\ & \times B_{\rm rf}^z(x\cos\delta_z - y\sin\delta_z). \quad (13)\end{aligned}$$

The additional component in Eq. (13) shows the spatial gradient of the potential along the direction of $x\cos\delta_z - y\sin\delta_z$. The direction of the gradient is a function of the relative phase δ_z and the amplitude of the gradient also linearly depends on the $B_{\rm rf}^z$. The additional rf field along the z axis tilts the ring potential along the direction of $x\cos\delta_z - y\sin\delta_z$ with an angle as a function of $B_{\rm rf}^z$.

Therefore, from Eqs. (11)–(13), we can control the asymmetry of the rf-induced potentials with the amplitude and relative phase shift of the rf field parallel to the local static field in the vicinity of the trap minima, $B^z_{\rm rf}$ and δ_z. This controllability can be understood as the result of modulating the coupling strength by changing the polarization of the rf field.

III. EXPERIMENTAL RESULTS

A. Atom chip for rf-induced potentials

For the experimental realization of rf-dressed potentials, atom chips are ideally suited since a large rf amplitude can be obtained by oscillating currents with relatively low amplitude in the chip wires. Figures 1(a) and 1(b) show the schematic of the atom chip used to realize the rf-induced potentials in our experiment. A dc current I^T_S in the trapping wire is used to produce an Ioffe-Pritchard trapping potential, and rf currents through rf wires with $\omega_{\rm rf}$, $I^A_{\rm rf}$, and $I^B_{\rm rf}$ provide the oscillating magnetic fields, $B^A_{\rm rf}$ and $B^B_{\rm rf}$. Static and oscillating currents through the dimple wire, I^D_S and $I^D_{\rm rf}$, are used to enhance the longitudinal confinement and control the asymmetry of the rf-induced potentials by manipulating an oscillating homogeneous field along the z direction, $B^z_{\rm rf}$, in the vicinity of the static potential minima. Figures 1(c) and 1(d) show the asymmetric double well and ring potentials calculated with the static Ioffe-Pritchard trap and the three-component rf field (2-kHz contours) for the typical set of experimental parameters $G = 50\,{\rm T/m}$, $B_I = 1$ G, $B_{\rm rf} = 1$ G, $B^z_{\rm rf} = 100$ mG, and $\omega_{\rm rf} = 2\pi \times 650$ kHz for ^{87}Rb atoms in the $F = m_F = 2$ hyperfine state. In the experiment we prepare a nearly pure BEC of $\sim 5 \times 10^4$ ^{87}Rb atoms in the $F = m_F = 2$ hyperfine state in a magnetic microtrap on the atom chip elongated along the z direction. The detailed apparatus and procedures we use for creating BEC are described elsewhere [34,35].

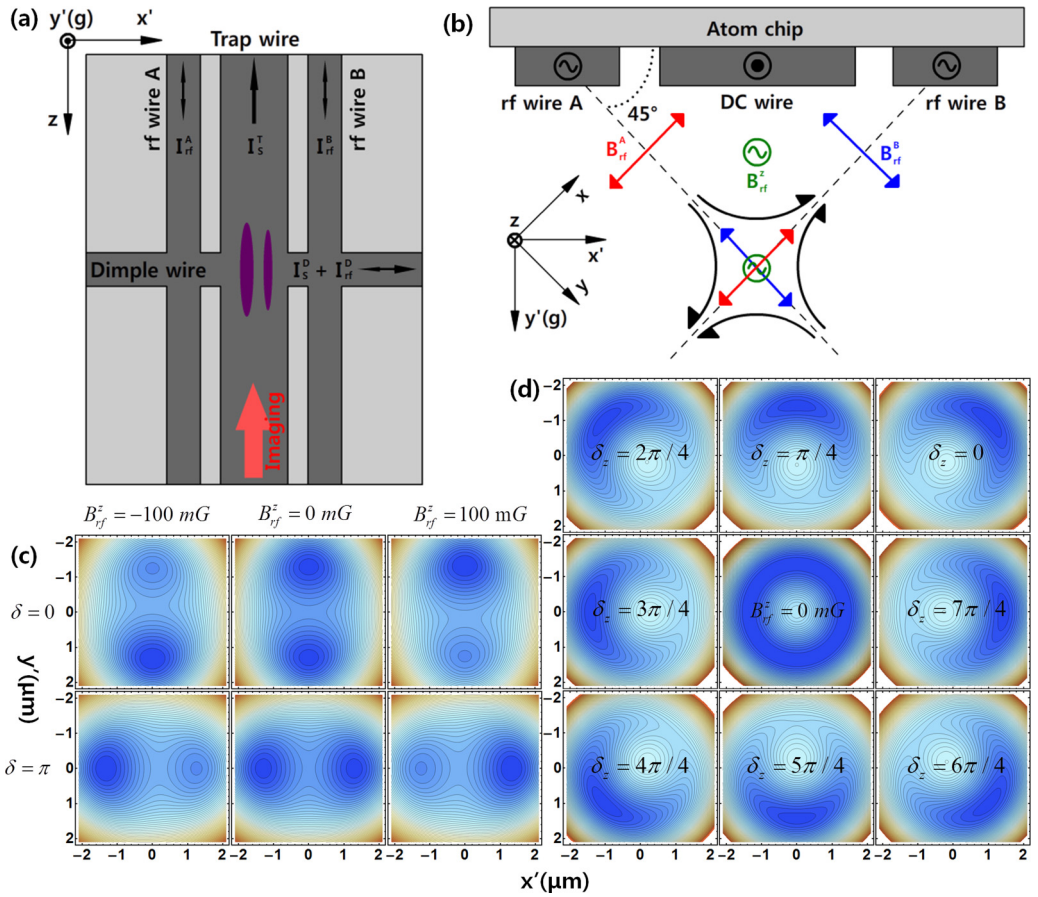

FIG. 1. (a,b) Schematic of the atom chip for asymmetric rf-induced potentials. (a) Top view of the four-wire setup. A broad (100-μm) central trap wire carrying a dc current is used with an external bias field to produce an Ioffe-Pritchard trapping potential. Smaller (50-μm) wires on each side separated by 102 μm from the trap wire provide the oscillating magnetic fields that create the adiabatic rf-induced potentials. Running dc currents through the dimple wire is used to enhance the longitudinal confinement, and rf currents control the asymmetry of the rf-induced potentials by manipulating the oscillating homogeneous field parallel to the quantization axis in the vicinity of the static potential minima. The atom distribution is imaged along the longitudinal axis of the trap by resonant absorption imaging. (b) Side view of the atom chip showing the relevant wires. The static trap is positioned such that the two rf fields from two rf wires are nearly perpendicular at its center. (c,d) Contour plot of the asymmetric rf-induced potentials with Ioffe-Pritchard static trap in the $z = 0$ plane (2-kHz contour). (c) Applying an additional rf field along the z direction can be used for controlling the asymmetry of the double-well potentials in both the vertical ($\delta = 0$) and horizontal ($\delta = \pi$) splitting cases. (d) Simulation of a tilted ring trap ($\delta = \pi/2$). The direction and the degree of the tilt are controlled by the relative phase δ_z and $B^z_{\rm rf}$, respectively.

B. Asymmetric double-well potential on atom chip

For the controllable asymmetric matter-wave beam splitter, the initial BEC is positioned 135 μm from the chip surface, with radial and axial trap frequencies of 866 and 26 Hz, respectively. The condensate is then split by using the three-component rf magnetic field produced by currents in the chip wires. The Larmor frequency at the static trap center is 700 kHz, and $\omega_{\rm rf}$ is fixed at a detuning of $2\pi \times 50$ kHz below this. By ramping up the rf amplitudes to the final $I_{\rm rf}^A = I_{\rm rf}^B = I_{\rm rf} \simeq 100$ mA (corresponding to $B_{\rm rf}^A = B_{\rm rf}^B \simeq 1180$ mG [36]), over 15 ms, which is sufficient to guarantee adiabaticity during the split, the asymmetric double well is formed.

The asymmetry of the double well can be investigated through observation of the relative atom number between the two wells [37] since simulations predict that the separation of the two minima, $\sim$4 μm, is far enough to prevent tunnel coupling [38]. Since the separation is beyond the resolution of our imaging system, we induced momentum on the atoms by quickly turning off the rf field ($<$1 μs), keeping the static magnetic trap turned on (referred to as the asymmetry-checking procedure in the following) [39]. The separated two clouds are accelerated by the gradient of the single well potential in the static trap. Since the fast turnoff projects the atoms onto the bare m_F states, the clouds from the two wells projected onto the $m_F = 1$ and 2 states are accelerated towards the static trap minima while the $m_F = 0$ atoms fall freely and the high-field-seeking atoms are rapidly expelled from the trap. After $\sim$800 μs, corresponding to three-fourths of a single harmonic trap period, the static trap is also switched off and then the clouds are separated far enough to be optically resolved with 2 ms time of flight. Figures 2(a) and 2(b) show the typical absorption images after the asymmetry-checking procedure for the horizontal ($\delta = \pi$) and vertical ($\delta = 0$) double well, respectively. The free-falling center cloud represents $m_F = 0$ states and the other clouds represent the $m_F = 1$ and 2 states. The high-field-seeking states are not shown in the images as they are expelled quickly from the static trap. The relative atom number between the two wells was determined by counting the numbers of atoms in the $m_F = 1$ and 2 states from each well. In addition, the positions of the two wells are deduced from the position measurements of the cloudlets in $m_F = 1$ and 2 states from each well [40].

The asymmetry of the double well is controlled by $I_{\rm rf}^D$. Figures 2(c) and 2(d) show the relative atom number between the two wells, $N_{m_F=1} + N_{m_F=2}$, as a function of the final $I_{\rm rf}^D$ in the range of our performance. The positions of the wells are almost unperturbed as the asymmetry is varied over a wide range, as expected from numerical calculations. Nonlinearity of the dependency in the case of a vertical double well arises from the downward sagging of the atoms due to gravity ($\Delta U = 2.1389$ kHz/μm). Since the effect of gravity causes a BEC to be trapped solely in the lower well, in previous studies, the position of the double well should be closer to the atom chip to achieve symmetric splitting [5,12,13]. However, in our scheme, symmetry is achieved with the proper choice of amplitude of $I_{\rm rf}^D$ for any position of the rf-induced double well.

C. Ring potentials on atom chip

The second case of interest is a ring potential on an atom chip. We were able to implement a ring potential on an atom chip by adjusting the asymmetry of the rf-induced potential. For the ring potential, the initial BEC is 102 μm directly below the trapping wire where the rf fields from the two rf wires are perpendicular to each other as given by Eq. (2), with radial and axial trap frequencies of 1367 and 34 Hz, respectively. The rf-induced potential forms a ring geometry for the trapped

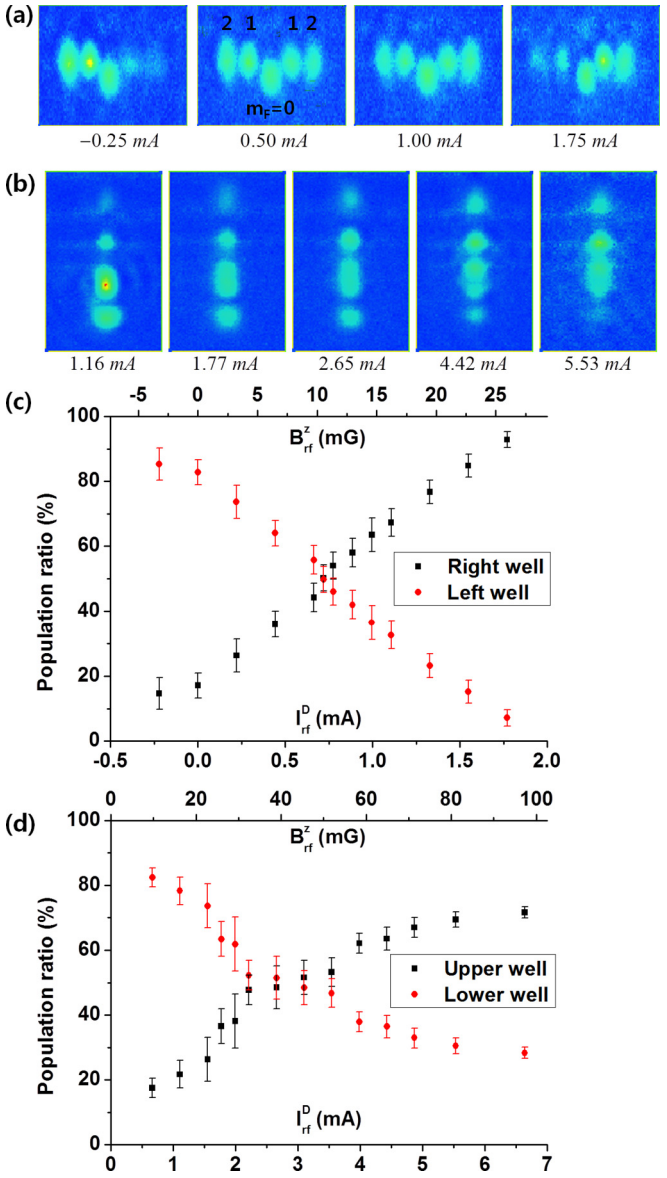

FIG. 2. Controllable asymmetric double-well potentials on an atom chip. The asymmetry is modulated with $I_{\rm rf}^D$ which manipulates the oscillating field along the z direction in the vicinity of the trap center. The positions of the wells are almost unperturbed as the asymmetry is varied over a wide range. (a,b) Images of the atoms from the double wells after the asymmetry-checking procedure (see text). The clouds on the left and right (top and bottom) wings are the atoms projected onto the $m_F = 1$ and 2 states from each well, with the $m_F = 0$ atoms positioned at the center. (c,d) Relative atom number between the two wells vs $I_{\rm rf}^D$. The population ratio is determined by counting the atoms in the $m_F = 1$ and 2 states from each well, $N_{m_F=1} + N_{m_F=2}$. Nonlinearity of the dependence in the case of the vertical double well arises from the downward sagging of the atoms due to gravity.

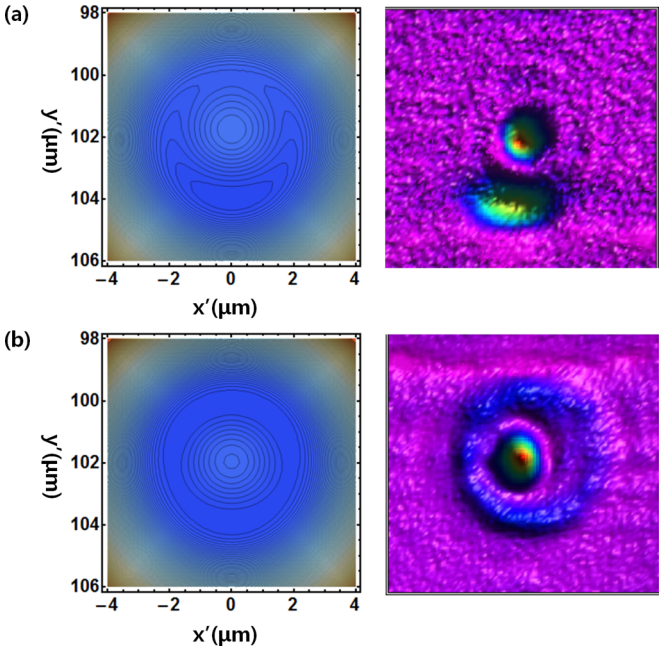

FIG. 3. Ring potential on an atom chip with $I_{\rm rf} = 57.5$ mA and $\delta = \pi/2$. Left: full numerical calculation with the exact wire geometry and parameters used in the experiments, including gravity (2-kHz contours). Right: image of a BEC in a ring trap after the asymmetry-checking procedure (the atoms in the center of the ring are in the $m_F = 0$ or high-field-seeking states). (a) Anisotropic ring potential due to gravity and inhomogeneous coupling strength of the rf field by the different distances from the rf wires, when $I^D_{\rm rf} = 0$. (b) Isotropic ring potential. The anisotropy is compensated by tilt of the ring potential with $I^D_{\rm rf} = 1.77$ mA and $\delta_z = \pi/4$.

atoms with $\delta = \pi/2$ and $I^A_{\rm rf} = I^B_{\rm rf} = I_{\rm rf}$. The $\omega_{\rm rf}$ and the ramping time are the same as those for the matter-wave beam splitter. The final $I_{\rm rf} = 57.5$ mA (corresponding to $B^A_{\rm rf} = B^B_{\rm rf} \simeq 797$ mG) is adjusted to achieve a ∼4-μm ring diameter, which is sufficiently confined to check the atom distribution via the asymmetry-checking procedure. As demonstrated in [5], the trapped atoms are positioned at the bottom of the ring potential due to gravity when $I^D_{\rm rf} = 0$ (corresponding to $B^z_{\rm rf} = 0$) [Fig. 3(a)]. The atoms in the center of the ring are $m_F = 0$ or high-field-seeking states, due to the spin flips that occur due to the turnoff of the rf fields as explained previously. We were able to confirm the nearly homogeneous atomic population around the ring with $I^D_{\rm rf} = 1.77$ mA (corresponding to $B^z_{\rm rf} = 34.0$ mG) and $\delta_z = \pi/4$, since these conditions tilt the ring potential opposite the direction of gravity, as numerically calculated with actual experimental conditions. Though the compensated ring potential has variations along the circumference of the ring, <1 kHz, the variation is less than the chemical potential of the trapped BEC, >2.6 kHz, which is given in [29] as $\mu_c = \hbar\bar{\omega}\sqrt{2Na/\pi r_0}$ (in the three-dimensional limit), where $\bar{\omega} = \sqrt{\omega_r \omega_z}$, $a = 100a_0$ is the scattering length (in units of the Bohr radius), r_0 is the radius, and N is the number of atoms in the ring trap. The difference between the potential variation and the chemical potential can be reduced since the potential variation can be reduced by decreasing the radius of the ring, while the chemical potential is a function of the controllable parameters, in particular ω_z, which can be controlled with I^D_S without perturbing the other parameters.

The tilt direction of the ring potential can also be controlled by changing the relative phase of the rf current through the dimple wire δ_z as expected from Eq. (13) [Figs. 4(a) and 4(b)]. The experimental results agree with the numerical calculation, and the maximal tilt is $< 5^\circ$, based on the actual atom chip dimensions and $I^D_{\rm rf} = 3.3$ mA (corresponding to $B^z_{\rm rf} = 63.5$ mG). The nonlinear response of the relative phase is due to gravity and anisotropic coupling strength of the rf fields.

In this manner, the angular velocity of the tilted ring potential can be controlled by changing the frequency difference Δf between $I_{\rm rf}$ and $I^D_{\rm rf}$, since the difference acts as a continuous change of δ_z with the phase velocity $2\pi\Delta f$ [41]. We measure the velocity of the trapped BECs in the rotating tilted ring potential by turning off the trapping fields after 1 ms rotating trap maintenance time. The inset of Fig. 4(c) shows the displacements of the untrapped atomic clouds from the initial position measured with 3 ms time of flight. Since the displacement is directly proportional to the induced velocity, by analyzing the displacements the velocities were measured as a function of the frequency differences [Fig. 4(c)]. As expected, the velocity is increased with the frequency difference. The frequency difference acts as a controlling knob for the angular momentum of the trapped atoms. Introducing controllable rotation into the system is necessary to study the dynamics of superfluidity in ring-trapped BECs.

IV. CONCLUSIONS

In conclusion, we have constructed a controllable asymmetric matter-wave beam splitter and a ring potential on an atom chip by dressing a static magnetic trap with a three-component rf field. By controlling the vector characteristics of the rf field, versatile controllability of the rf-induced potentials was obtained. Asymmetry of the rf-induced double well is manipulated without discernible displacement of each well. The controllability of the asymmetry will be a useful tool for atom interferometry since it can be used to compensate any position-dependent asymmetry in a matter-wave beam splitter [10,37] or act as a phase shifter [18]. Dynamical behaviors of superfluids, such as Josephson dynamics [17,19,20,42], can also be a subject of study in our scheme due to the precise modulation of the bias between two wells. Formation of an isotropic ring potential on an atom chip is achieved by compensating the gradient due to gravity and inhomogeneous coupling strength. In addition, the position and velocity of a BEC along the ring geometry are controlled by the relative phase and the frequency difference between the rf fields, respectively. Realizing ultracold atoms in the strongly correlated fractional quantum Hall regime has been a long-term goal of the research community [43,44]. The smooth modification between a ring-shaped and harmonic trap, attainable very-low-energy scale of the system, and controllable versatility of the potential allowing the dynamics of the atomic system covering its angular momentum with a high degree of accuracy are the most prominent characteristics for this goal [45–47].

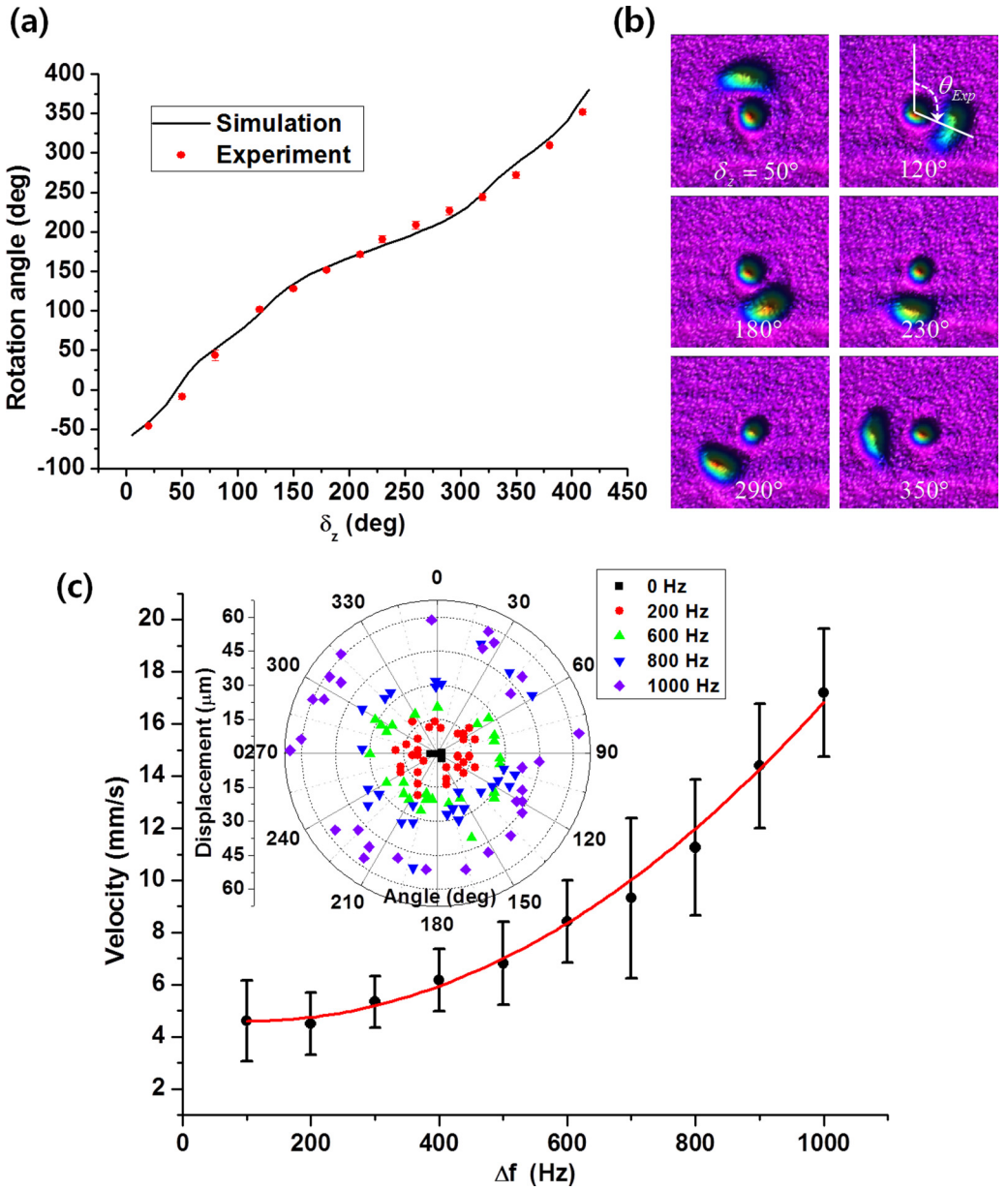

FIG. 4. (a,b) The direction of the tilt vs the relative phase of the rf current through the dimple wire, δ_z. (a) The experimental results and expected values from the simulations using actual experimental parameters. (b) Typical absorption images of a BEC in a tilted ring trap after the asymmetry-checking procedure. The angle in the picture represents δ_z. (c) Velocity of a BEC in a rotating tilted ring trap. The angular velocity of the tilted ring potential has been controlled with the frequency difference between I_{rf} and I_{rf}^{D}. To confirm that the frequency difference induces rotation on a BEC, the rotating tilted trap turned off after 1 ms. The solid line is a polynomial fitting curve. The inset shows the displacements of the BECs after turning off the trap and 3 ms time of flight.

ACKNOWLEDGMENTS

This work was supported by a grant to the Atom Optic Sensor Laboratory for National Defense funded by DAPA/ADD and by Basic Science Research Program through the National Research Foundation of Korea (NRF) funded by the Ministry of Science, ICT & Future Planning (Grant No. 2014R1A2A2A01007460).

[1] J. Fortágh and C. Zimmermann, Rev. Mod. Phys. **79**, 235 (2007).

[2] O. Zobay and B. M. Garraway, Phys. Rev. Lett. **86**, 1195 (2001).

[3] Y. Colombe, E. Knyazchyan, O. Morizot, B. Mercier, V. Lorent, and H. Perrin, Europhys. Lett. **67**, 593 (2004).

[4] I. Lesanovsky, T. Schumm, S. Hofferberth, L. M. Andersson, P. Krüger, and J. Schmiedmayer, Phys. Rev. A **73**, 033619 (2006).

[5] S. Hofferberth, I. Lesanovsky, B. Fisher, J. Verdu, and J. Schmiedmayer, Nat. Phys. **2**, 710 (2006).

[6] I. Lesanovsky and W. von Klitzing, Phys. Rev. Lett. **99**, 083001 (2007).

[7] W. H. Heathcote, E. Nugent, B. T. Sheard, and C. J. Foot, New J. Phys. **10**, 043012 (2008).

[8] T. Schumm, S. Hofferberth, L. M. Andersson, S. Wildermuth, S. Groth, I. Bar-Joseph, J. Schmiedmayer, and P. Krüger, Nat. Phys. **1**, 57 (2005).

[9] T. Berrada, S. van Frank, R. Bücker, T. Schumm, J.-F. Schaff, and J. Schmiedmayer, Nat. Commun. **4**, 2077 (2013).

[10] F. Baumgärtner, R. J. Sewell, S. Eriksson, I. Llorente-Garcia, J. Dingjan, J. P. Cotter, and E. A. Hinds, Phys. Rev. Lett. **105**, 243003 (2010).

[11] G.-B. Jo, J.-H. Choi, C. A. Christensen, T. A. Pasquini, Y.-R. Lee, W. Ketterle, and D. E. Pritchard, Phys. Rev. Lett. **98**, 180401 (2007).

[12] S. Hofferberth, I. Lesanovsky, B. Fischer, T. Schumm, and J. Schmiedmayer, Nature **449**, 324 (2007).

[13] M. Gring, M. Kuhnert, T. Langen, T. Kitagawa, B. Rauer, M. Schreitl, I. Mazets, D. Adu Smith, E. Demler, and J. Schmiedmayer, Science **337**, 1318 (2012).

[14] G.-B. Jo, Y. Shin, S. Will, T. A. Pasquini, M. Saba, W. Ketterle, D. E. Pritchard, M. Vengalattore, and M. Prentiss, Phys. Rev. Lett. **98**, 030407 (2007).

[15] G.-B. Jo, J.-H. Choi, C. A. Christensen, Y.-R. Lee, T. A. Pasquini, W. Ketterle, and D. E. Pritchard, Phys. Rev. Lett. **99**, 240406 (2007).

[16] M. F. Riedel, P. Böhl, Y. Li, T. W. Hänsch, A. Sinatra, and P. Treutlein, Nature **464**, 1170 (2010).

[17] L. J. LeBlanc, A. B. Bardon, J. McKeever, M. H. T. Extavour, D. Jervis, J. H. Thywissen, F. Piazza, and A. Smerzi, Phys. Rev. Lett. **106**, 025302 (2011).

[18] S. van Frank, A. Negretti, T. Berrada, R. Bücker, S. Montangero, J.-F. Schaff, T. Schumm, T. Calarco, and J. Schmiedmayer, Nat. Commun. **5**, 4009 (2014).

[19] S. Levy, E. Lahoud, I. Shomroni, and J. Steinhauer, Nature **449**, 579 (2007).

[20] M. Albiez, R. Gati, J. Fölling, S. Hunsmann, M. Cristiani, and M. K. Oberthaler, Phys. Rev. Lett. **95**, 010402 (2005).

[21] S. Gupta, K. W. Murch, K. L. Moore, T. P. Purdy, and D. M. Stamper-Kurn, Phys. Rev. Lett. **95**, 143201 (2005).

[22] C. Ryu, M. F. Andersen, P. Cladé, V. Natarajan, K. Helmerson, and W. D. Phillips, Phys. Rev. Lett. **99**, 260401 (2007).

[23] P. M. Baker, J. A. Stickney, M. B. Squires, J. A. Scoville, E. J. Carlson, W. R. Buchwald, and S. M. Miller, Phys. Rev. A **80**, 063615 (2009).

[24] K. Henderson, C. Ryu, C. MacCormick, and M. G. Boshier, New J. Phys. **11**, 043030 (2009).

[25] B. E. Sherlock, M. Gildemeister, E. Owen, E. Nugent, and C. J. Foot, Phys. Rev. A **83**, 043408 (2011).

[26] A. Ramanathan, K. C. Wright, S. R. Muniz, M. Zelan, W. T. Hill III, C. J. Lobb, K. Helmerson, W. D. Phillips, and G. K. Campbell, Phys. Rev. Lett. **106**, 130401 (2011).

[27] S. Moulder, S. Beattie, R. P. Smith, N. Tammuz, and Z. Hadzibabic, Phys. Rev. A **86**, 013629 (2012).

[28] S. Beattie, S. Moulder, R. J. Fletcher, and Z. Hadzibabic, Phys. Rev. Lett. **110**, 025301 (2013).

[29] O. Morizot, Y. Colombe, V. Lorent, H. Perrin, and B. M. Garraway, Phys. Rev. A **74**, 023617 (2006).

[30] A. J. Legett, Rev. Mod. Phys. **73**, 307 (2001).

[31] C. Ryu, P. W. Blackburn, A. A. Blinova, and M. G. Boshier, Phys. Rev. Lett. **111**, 205301 (2013).

[32] P. F. Griffin, E. Riis, and A. S. Arnold, Phys. Rev. A **77**, 051402 (2008).

[33] K. C. Wright, R. B. Blakestad, C. J. Lobb, W. D. Phillips, and G. K. Campbell, Phys. Rev. Lett. **110**, 025302 (2013).

[34] H. Yu, S. J. Kim, Y. L. Moon, J. S. Lee, and J. B. Kim, J. Korean Phys. Soc. **63**, 900 (2013).

[35] S. J. Kim, J. J. Noh, M. S. Kim, J. S. Lee, H. Yu, and J. B. Kim, J. Opt. Soc. Korea **18**, 633 (2014).

[36] There is little variation of the axis notation in Eq. (2) due to the distance from the chip surface, 135 μm, which is far from the position with the distance 102 μm where the rf fields from the two rf wires are perpendicular to each other as given by Eq. (2).

[37] B. V. Hall, S. Whitlock, R. Anderson, P. Hannaford, and A. I. Sidorov, Phys. Rev. Lett. **98**, 030402 (2007).

[38] S. Raghavan, A. Smerzi, S. Fantoni, and S. R. Shenoy, Phys. Rev. A **59**, 620 (1999).

[39] T. Schumm, Bose-Einstein condensates in magnetic double well potentials, Ph.D. thesis, University of Paris Sud, University of Heidelberg, 2005.

[40] The center positions of the atom clouds are determined via two-dimensional Gaussian fitting and used for deducing the positions of the two rf-induced wells.

[41] See Supplemental Material at http://link.aps.org/supplemental/10.1103/PhysRevA.93.033612 for simulation results of both rotating and ring potentials as well as the movie using absorption images.

[42] J. Ground, T. Betz, U. Hohenester, N. J. Mauser, J. Schmiedmayer, and T. Schumm, New J. Phys. **13**, 065026 (2011).

[43] N. R. Cooper, N. K. Wilkin, and J. M. F. Gunn, Phys. Rev. Lett. **87**, 120405 (2001).

[44] A. L. Fetter, Rev. Mod. Phys. **81**, 647 (2009).

[45] S. Viefers, J. Phys.: Condens. Matter **20**, 123202 (2008).

[46] M. Roncaglia, M. Rizzi, and J. Dalibard, Sci. Rep. **1**, 43 (2011).

[47] M. Gildemeister, B. E. Sherlock, and C. J. Foot, Phys. Rev. A **85**, 053401 (2012).